Bioorganic Chemistry 84 (2019) 372–383

Contents lists available at ScienceDirect

Bioorganic Chemistry

journal homepage: www.elsevier.com/locate/bioorg

Xanthenone-based hydrazones as potent α-glucosidase inhibitors: Synthesis, solid state self-assembly and in silico studies

Qamar-un-Nisa Tariq[a], Sana Malik[b], Ajmal Khan[c], Muhammad Moazzam Naseer[d], Shafi Ullah Khan[e], Abida Ashraf[a,f], Muhammad Ashraf[b], Muhammad Rafiq[a], Khalid Mahmood[a], Muhammad Nawaz Tahir[g], Zahid Shafiq[a,*]

[a] Institute of Chemical Sciences, Bahauddin Zakariya University, Multan 60800, Pakistan
[b] Department of Chemistry, The Islamia University of Bahawalpur, Bahawalpur 63100, Pakistan
[c] Natural and Medical Sciences Research Center, University of Nizwa, P.O. Box 33, Birkat Al Mauz, Nizwa 616, Oman
[d] Department of Chemistry, Quaid-i-Azam University, Islamabad 45320, Pakistan
[e] School of Pharmacy, Monash University Malaysia, Jalan Lagoon Selatan, Bandar Sunway, 47500 Subang Jaya, Selangor, Malaysia
[f] Department of Chemistry, The Woman University, Multan, Pakistan
[g] Department of Physics, University of Sargodha, Sargodha, Pakistan

ARTICLE INFO

Keywords:
Xanthenone
Hydrazone
α-glucosidase inhibitor
Acarbose
Molecular docking study

ABSTRACT

Xanthenone based hydrazone derivatives **(5a–n)** have been synthesized as potential α-glucosidase inhibitors. All synthesized compounds **(5a–n)** are characterized by their FTIR, ^{1}H NMR, ^{13}C NMR and HRMS, and in case of **5g** also by X-ray crystallographic technique. The compounds unveiled a varying degree of α-glucosidase inhibitory activity when compared with standard acarbose (IC_{50} = 375.38 ± 0.12 μM). Amongst the series, compound **5l** (IC_{50} = 62.25 ± 0.11 μM) bearing a trifluoromethyl phenyl group is found to be the most active compound. Molecular modelling is performed to establish the binding pattern of the more active compound **5l,** which revealed the significance of substitution pattern. The pharmacological properties of molecules are also calculated by MedChem Designer which determines the ADME (absorption, distribution, metabolism, excretion) properties of molecules. The solid state self-assembly of compound **5g** is discussed to show the conformation and role of iminoamide moiety in the molecular packing.

1. Introduction

Diversity oriented synthesis and cyclization reactions continues to grow powerful stratagem in organic synthesis and has inspired advances in drug designing and synthesis of compounds having natural product skeleton [1]. The synthesis of xanthene and its derivatives have gained prodigious attention in the last few decades due to their prominent position in medicinal chemistry. Xanthenes and benzoxanthenes exhibit diverse pharmaceutical activities such as antiviral [2,3] **1**, antidiabetic [4] **2**, antibacterial [5–8] **3**, antiplasmodial **4** and antioxidant [9–11] **5**. Furthermore, xanthene and their derivatives due to interesting spectroscopic properties have been used as dyes [12] and in laser technology [13] (Fig. 1).

Furthermore, xanthene derivatives have been reported as charge-control agent in electrophotographic toner [13], pH sensitive fluorescent material for the visualization of biomolecules and as marker or biological stains [14]. Rhodamine and rosamine particularly have been used in ink for ink-jet printers [15]. These compounds have also been investigated for photodynamic therapy, anti-inflammatory effects [16] and agricultural bactericidal activity [17]. A number of xanthene derivatives are the structural motifs of naturally occurring compounds, as santalin pigments have been isolated from a number of plant species [18].

Hydrazones constitute versatile class of compounds in heterocyclic chemistry and possess potential biological activities such as antioxidant [19], anticonvulsive [20], antitumor [21], anti-inflammatory [22], antiviral [23], antimicrobial [24,25] and analgesic [26]. The inclusive medicinal importance associated with xanthenes and hydrazones both naturally occurring and synthetic, confirm that the synthesis of these compounds remains a topic of current interest. Diabetes mellitus is one of the most common metabolic disease worldwide and consists of several types, one of which is noninsulin dependent diabetes mellitus (type 2 DM). This increasing trend in type 2 DM, has become a serious medical concern worldwide that prods every exertion in reconnoitering

* Corresponding author.
E-mail address: zahidshafiq@bzu.edu.pk (Z. Shafiq).

https://doi.org/10.1016/j.bioorg.2018.11.053
Received 15 October 2018; Received in revised form 27 November 2018; Accepted 29 November 2018
Available online 30 November 2018
0045-2068/

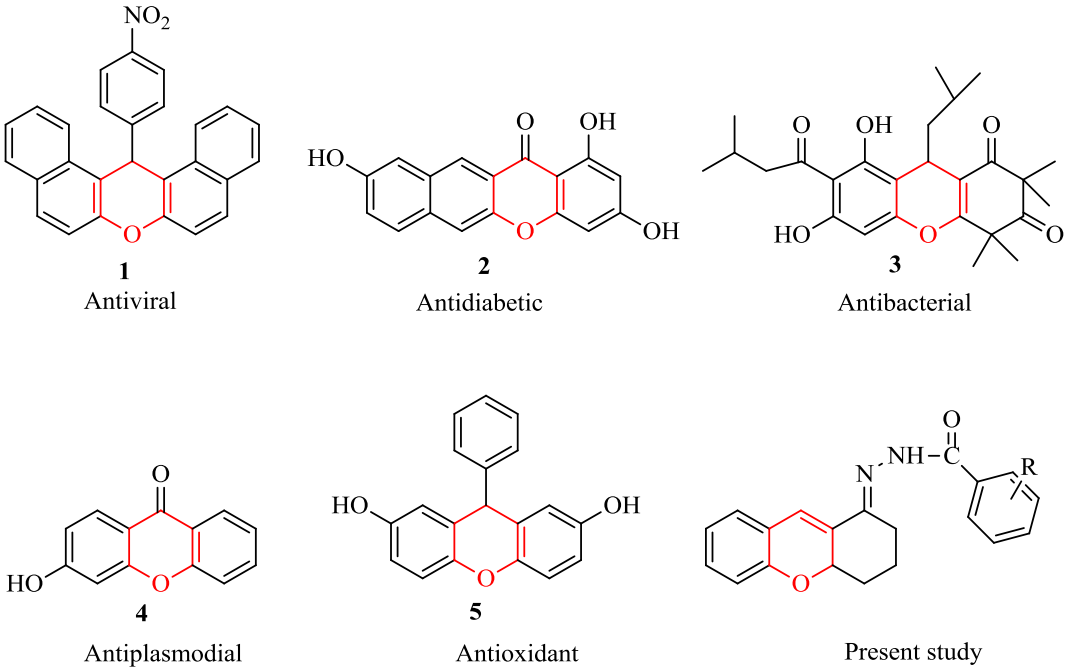

Fig. 1. Biologically active Xanthenes.

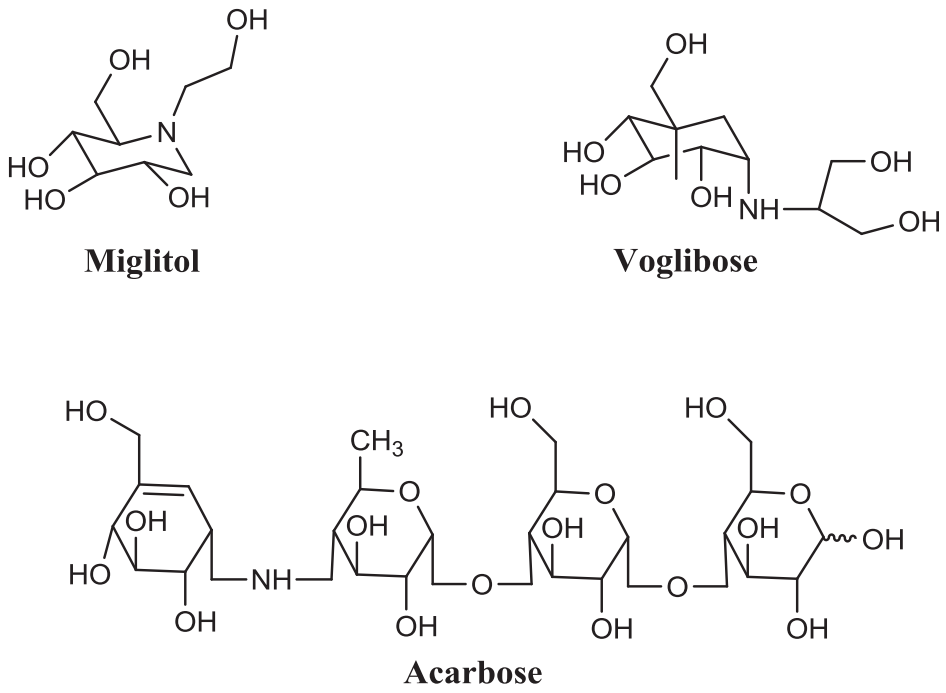

Fig. 2. Some commercial anti-diabetic drugs.

for new therapeutic agents to stem its progress [27]. It has been reported that diabetes mellitus will affect 300 million people worldwide by 2025 [28]. More than 90% of the patients possess diabetes mellitus type-2 [29] which is a metabolic disorder showing hyperglycemia either due to insulin resistance or relative insulin deficiency. Its symptoms include excessive thirst, hunger and urination. There are many approaches to manage hyperglycemia and one such way is to inhibit the activity of α-glucosidase (EC.3.2.1.20) enzyme produced by the brush border of small intestine. It causes hydrolysis of α-1–4 glycoside bond in oligosaccharides to produce glucose which is absorbed and is responsible for post-prandial hyperglycemia in diabetic patients [30]. The inhibitors of this enzyme include Acarbose, Voglibose and Miglitol (Fig. 2) which are used as antidiabetic drugs in the market but cause flatulence, diarrhea and abdominal discomfort [31]. Therefore, to overcome side effects, there is always need of α-glucosidase inhibitors. The present studies are a perpetuation of our work in search for lead compounds inhibiting the said enzyme.

Thus, in continuation of our drug discovery research [32–35], present study is to synthesize a novel series of hydrazones of 2,3,4,4a tetrahydroxanthene-1-one and screen them mainly for their in vitro α-glucisidase inhibition activity. This study is one of the first to report on hydrazones of 2,3,4,4a tetrahydroxanthene-1-one with α-glucisidase inhibitory potential.

Table 1
2,3,4,4a-tetrahydro-1H-xanthen-1-ylidene)benzohydrazide (**5a–n**).

Compound no.	R	Yield (%)	Compound no.	R	Yield (%)
5a		84	**5h**	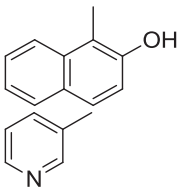	88
5b	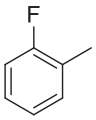	72	**5i**		80
5c	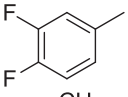	78	**5j**	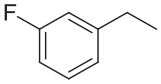	73
5d	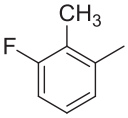	85	**5k**	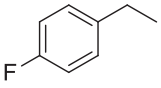	85
5e	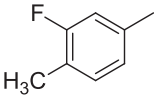	80	**5l**	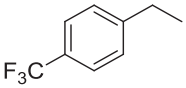	82
5f	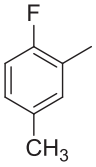	65	**5m**	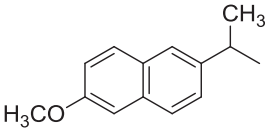	90
5g	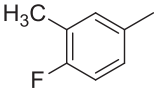	79	**5n**	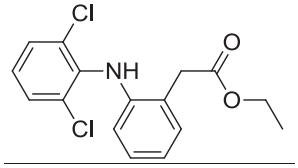	81

2. Results and discussion

2.1. Chemistry

To investigate the potential of xanthene based hydrazones (**5a–n**), a series of substituted hydrazide (**4a–n**) were taken to react with 2,3,4,4*a*-tetrahydroxanthen-1-one (**3**) prepared by previously reported methodology [32]. A typical condensation method was instigated by treating appropriate hydrazides (**4a–n**) with xanthene (**3**). The reaction was carried out in ethanol by using catalytic amount of glacial acetic acid (1–2 drops). The optimization of reaction conditions was done by treating phenylhydrazide (**4a**) with xanthene (**3**) in equimolar amounts by using solvents of variable polarity i.e. ethanol, methanol, DCM, THF and DMSO. The optimum conditions were established by refluxing the reaction mixture in the presence of ethanol as solvent and by employing glacial acetic acid as catalyst. The scope of reaction was extended vide reacting xanthene (**3**) with assortment of hydrazides (**1a-p**). The targeted hydrazones (**5a–n**) were obtained in good to excellent yields (**65–90%**) (Table 1) (see Scheme 1).

The structures of novel hydrazones derived from xanthene (**3**) were established by using spectroscopic techniques i.e. IR, ^{1}H NMR, ^{13}C NMR and mass spectrometry. The stretching of N—H band of hydrazone moiety in FTIR appeared in the range of 3205–3378 cm^{-1} whereas amidic C=O stretching was observed between 1647 and 1687 cm^{-1} affirming the formation of new C=N (azomethine) linkage in hydrazones (**5a–n**). In ^{1}H NMR spectra (recorded in $CDCl_3$), NH—N=C appeared in the range from δ 7.44–7.82 ppm while in DMSOd_6, it appeared as singlet ranging from δ 10.61–11.75 ppm. The HRMS was also taken to endorse the molecular mass of the synthesized derivatives (**5a–n**) and was found to be in good agreement with the calculated values. The spectral data of other aromatic and aliphatic protons was also in accordance with the structures of predicted compounds. The mass fragmentation pattern of a representative compound **(5j)** is also shown in (Fig. 3). The structure of the xanthene based hydrazone was also established by taking single crystal X-ray of (**5g**).

2.2. X-ray crystallographic studies

The single crystals of compound **5g** for X-ray diffraction analysis were grown in solvent by its slow evaporation. The compound **5g** crystallizes in orthorhombic crystal lattice with the *Pbca* space group. The molecular structure (ORTEP diagram) of compound **5g** containing crystallographic numbering is presented in Fig. 4. In the crystal structure, the central *N*-iminoamide moiety is nearly planar having the aryl and tetrahydroxanthene moieties tilted from the plane. The dihedral angles between C(16)—C(15)—C(14)—O(2) and C(8)—C(13)—N(1)—N(2) are −142.21° and −176.70°, respectively. The planarity of central iminoamide moiety can be attributed to the delocalized nitrogen electrons onto the amide as well as to the imino moiety, which is clearly evidenced by the bond lengths between N—C [N(2)—C(14) 1.357 Å] and N—N [N(2)—N(1) 1.386 Å]. In contrast to the previously highlighted *cis*-conformation of thioamides of thiosemicarbazones [32,36], the central amide moiety in compound **5g** is present in *trans*-conformation. Hence, the centrosymmetric amide dimer $R_2^2(8)$ $(\cdots H-N-C=O)_2$ synthon is absent in the packing of compound **5g** (Fig. 4).

The molecules in 3D packing of compound **5g** are arranged at nearly right angle to each other making 1D-supramolecular chains (Fig. 5a). The main intermolecular interactions include NH···O (N(2)—H(2A)···O

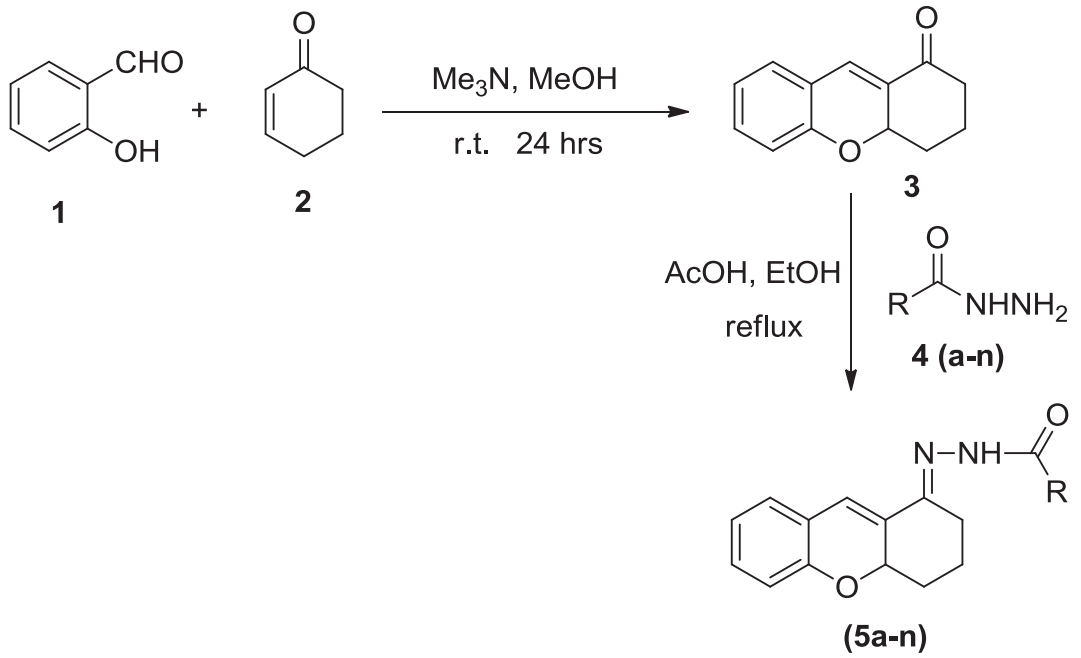

Scheme 1. Synthesis of 2,3,4,4*a*-tetrahydroxanthen-1-one 3 and its hydrazone derivatives.

(2) 2.621 Å), NH···N (N(2)—H(2A)···N(1) 2.551 Å) and CH···O (C(21)—H(21C)···O(2) 2.636 Å & C(16)—H(16)···O(2) 2.588 Å). The 1D-supramolecular chains are connected to the neighbouring chains by means of CH—F (C(21)—H(21A)···F(1) 2.520 Å) interaction providing an overall 3D-network structure [37] (Fig. 5b and c).

2.3. α-glucisidase inhibitory activity

The inhibitory activity of Xanthene derivatives **(5a–n)** towards yeast α-glucisidase was measured [38–40] and the mainstream of compounds unveiled a varying degree of α-glucosidase inhibitory activity with IC_{50} values when equated with standard acarbose (IC_{50} = 375.38 ± 0.12 μM) and the results are summarized in Table 2. Among the series, compounds **5l, 5g, 5j, 5n and 5m** were found to be most active α-glucisidase inhibitor with IC_{50} value of 62.25 ± 0.11, 79.25 ± 0.15, 95.48 ± 0.13, 96.48 ± 0.53 and 96.54 ± 0.57 μM, while in pool of remaining compounds **5b, 5d, 5k** showed loss of inhibitory activity. The overall order of α-glucosidase inhibition activity of compounds **(5a–n)** was as follows:

5l* > *5g* > *5j* > *5n* > *5m* > *5f* > *5c* > *5h* > *5a* > *5e* > *5i* > *5b* > *5d* > *5k

2.4. Structure-activity relationship

The SAR of compounds **(5a–n)** have been described by the presence of electron donating and withdrawing groups. The presence of electron withdrawing groups on ortho, meta and para positions of phenyl ring such as trifluoromethyl and fluorine results in an increase and decrease in inhibitory activity of compounds (Table 2). The compound **5l** containing trifluoromethyl group at the para position of the phenyl ring exhibited potent α-glucosidase inhibitory activity with IC_{50} value of 62.25 ± 0.11 μM. The second most active compound **5g** (IC_{50} = 79.25 ± 0.15 μM) have fluorine moiety at para position indicating that electron withdrawing groups at para position may be responsible for increased in activity. This compound have also methyl group at para position, which decreased their activity. The activity of this compound little further decreased, when this fluorine moiety shift to meta position as observed in compound **5e** (IC_{50} = 79.25 ± 0.15 μM). The activity further 5 time decreased, when methyl group shift to ortho as observed in compound **5d** (IC_{50} = 317.12 ± 0.12 μM), which may be produced steric hindrance in the interaction of this compound with enzyme active site. The compound **5j** bearing fluorine at meta position also showed good activity with IC_{50} value of 95.48 ± 0.13 μM. The activity of this compounds decrease when another fluorine was substituted at para position as in compound **5c** (IC_{50} = 124.58 ± 0.15 μM), while the activity 3 time decreased, when fluorine shifted to ortho position (compound **5b**) The binding interactions of molecule into active site of α-glucosidase were elucidated by molecular docking studies.

2.5. In silico Studies

2.5.1. Homology model of S. cerevisiae α-glucosidase

The 3D structure of α-glucosidase is required for molecular docking studies. For this purpose, first homology modelled 3D structure of the target *S. cerevisiae* α-glucosidase was made. The sequence alignments between isomaltase from *S. cerevisiae* (PDB ID: 3A4A) and *S. cerevisiae* α-glucosidase showed that there was high sequence identity and sequence similarity of 71.4% and 86.9%, respectively. Crystal structure of isomaltase from *S. cerevisiae* was selected as template structure and downloaded from protein databank. Twenty different modelled structures were built and based on DOPE score, the best model was selected. Validation of modelled structure was performed via Ramachandran plot and showed that about 98.1% residues were in favoured region, 1.9% residues were in allowed region while no outlier residue was found in structure (Table 3). It indicated the good stereochemistry of modelled structure and was found fit for further docking studies. 3D overlapped structure of template structure and modelled structure of α-glucosidase are shown in Fig. 6 while Ramachandran plot is shown in Fig. 7.

2.5.2. Molecular Docking Studies

To validate the docking protocol, first bound co-crystal ligand the α-D-glucose was docked in the modelled structure which exhibited very good RMSD of 0.73 (Fig. 8). It shows the crystal and re-docked α-D-glucose within the active site of target structure. Fig. 9 shows the overlapped binding orientation of all docked compounds within the active site of modelled structures. Docking of all compounds within the active site showed that all compounds were docked well within the

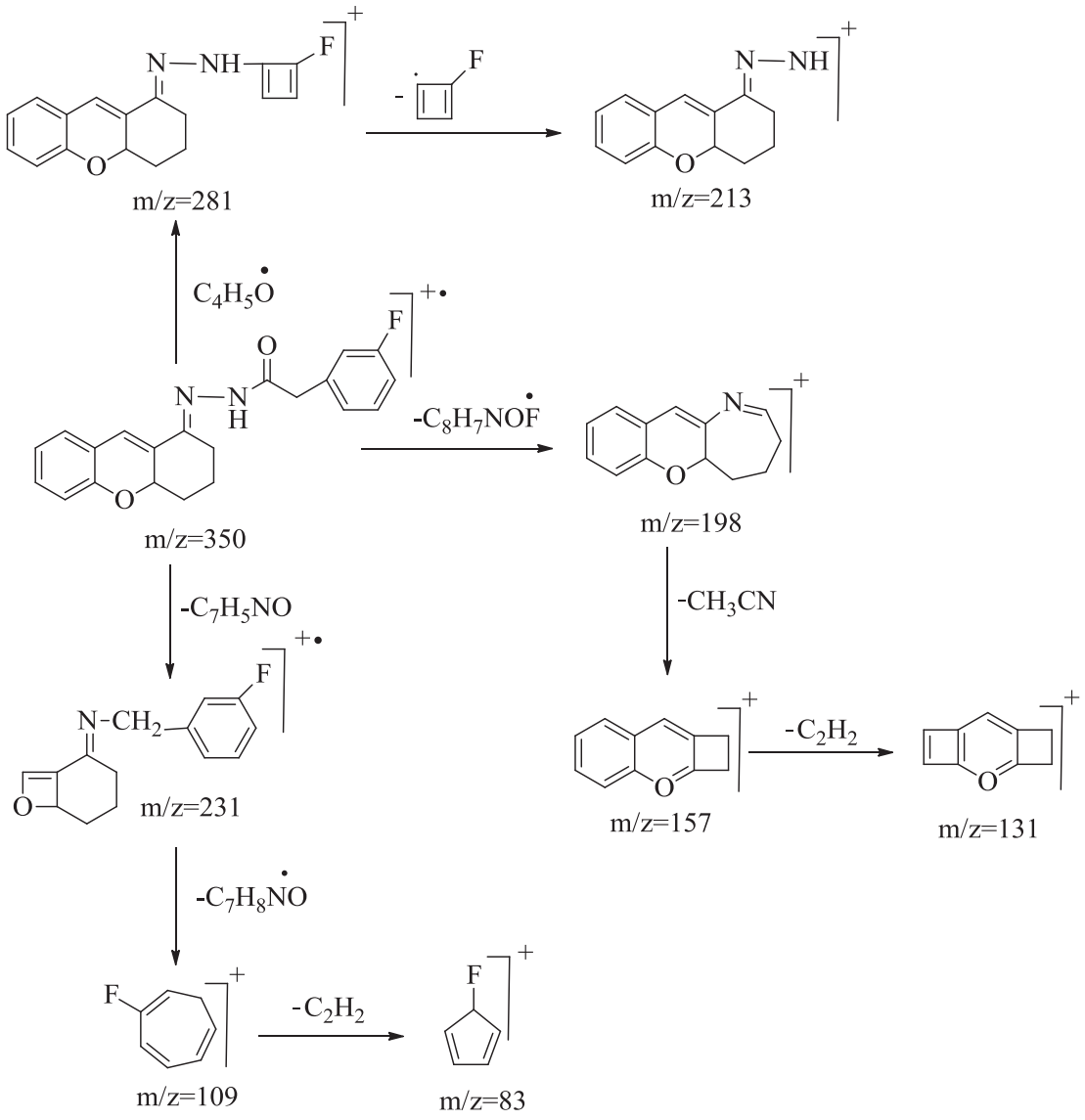

Fig. 3. The proposed MS fragmentation pattern of compound **5j**.

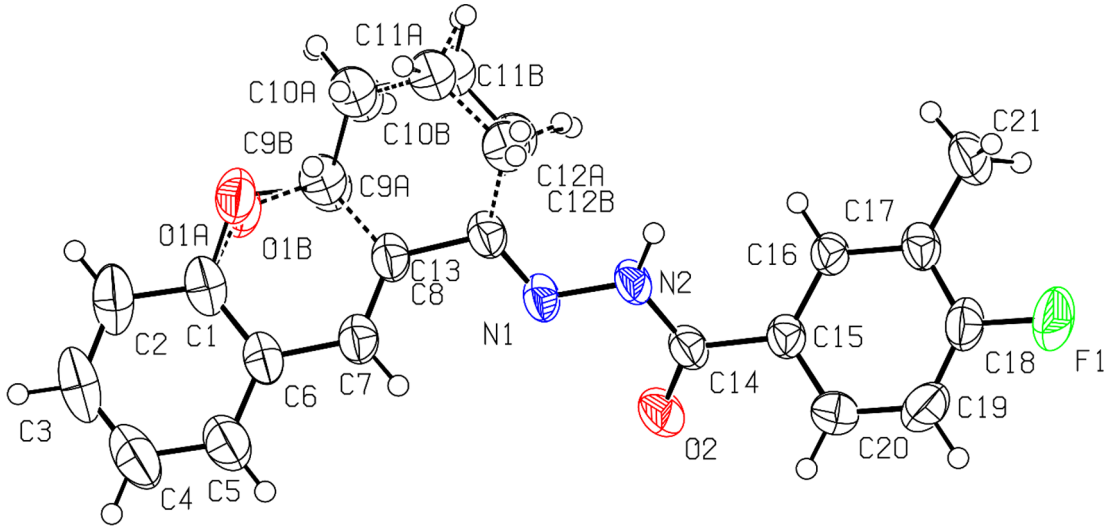

Fig. 4. The molecular structure (ORTEP diagram) of compound **5g**.

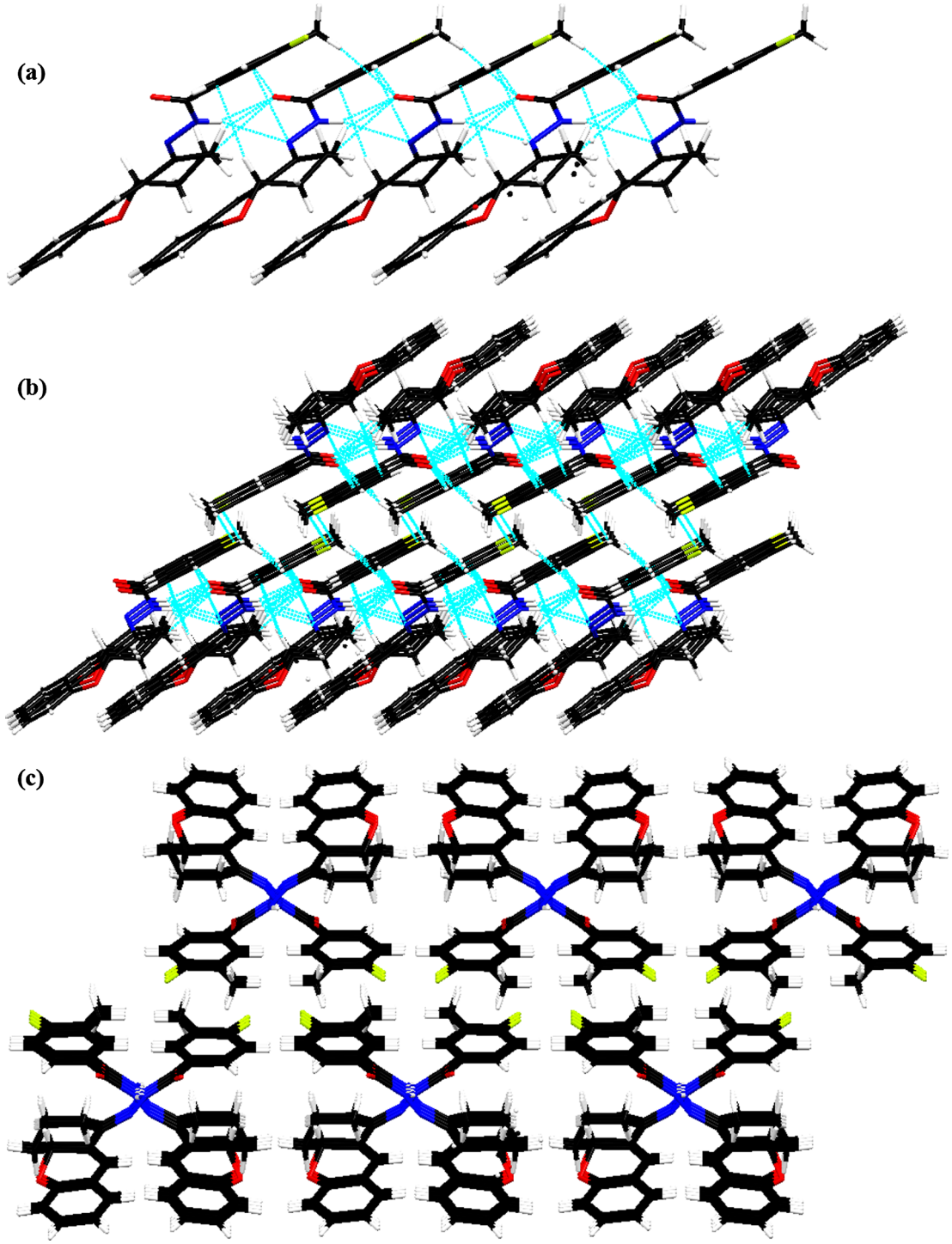

Fig. 5. Molecular packing of compound **5g**: (a) showing 1D-supramolecular chains along a-axis; (b) showing 3D-network structure along a-axis; (c) showing 3D-network structure along b-axis.

active site of target enzymes (Fig. 9) and ChemGauss4 score of docked compounds is shown in Table 4. Differences in binding interactions were due to the attached side chain differences in corresponding compounds. Detailed analysis of binding interactions of potent compounds, for example **5l**, which showed relatively higher inhibitory potential than the other tested compounds, exhibited ChemGauss4 score of −11.478. Different amino acid residues of target enzyme were involved in making binding interactions with side chains of compound **5l** (Fig. 10). Amino acid residues Thr215 and Glu276 were involved in forming two hydrogen bonds with the two nitrogen atoms of the hydrazine moiety as shown in green dotted line. Fluorine atoms were involved in forming halogen interaction with amino acid residues Arg312, Asp408 and Phe157, as shown in cyan dotted line in (Fig. 10). Amino acid Phe300 was also involved in making pi-pi stacked with fused benzene moiety of compound **5l** as shown in pink dotted line. Other hydrophobic interactions were formed between amino acid residues Phe300 and Phe157 and pyran and cyclohexane moiety of compound as shown in (Fig. 11).

Table 2
Yeast anti-α-glucosidase activity. Data is mean of three values (mean ± s.e.m., n = 3).

Compound	IC_{50} (μM ± SEM)	Compound	IC_{50} (μM ± SEM[a])
5a	148.26 ± 0.14	**5h**	138.25 ± 0.13
5b	316.34 ± 0.12	**5i**	157.26 ± 0.17
5c	124.58 ± 0.15	**5j**	95.48 ± 0.13
5d	317.12 ± 0.12	**5k**	317.28 ± 0.18
5e	153.26 ± 0.19	**5l**	62.25 ± 0.11
5f	123.29 ± 0.13	**5m**	96.54 ± 0.57
5g	79.25 ± 0.15	**5n**	96.48 ± 0.53
Acarbose	**375.38 ± 0.12**		

Table 3
Ramachandran plot analysis of *S. cerevisiae* α-glucosidase.

Favoured region	Allowed region	Outlier region
569 (98.1%)	11 (1.9%)	0 (0.0%)

Fig. 6. 3D overlapped orientation of template structure (PDB: 3A4A in green colour) superimposed on modelled structure of α-glucosidase in (purple colour).

2.6. ADME properties of compounds

The pharmacological properties of molecules were calculated by MedChem Designer [41], which determines the ADME (absorption, distribution, metabolism, excretion) properties of molecules (Table 5). It is shown that the computational methods could be used for the prediction of intestinal drug permeability in rats as does the experimental methods. Amongst the calculated parameters, higher logD and logP values and lower number of hydrogen bonds predict higher bioavailability of drugs. TPSA is the topological polar surface area expressed in square angstroms. A molecule with TPSA value of < 60 Å^2 exhibits sufficient bioavailability whilst if this value exceeds 140 Å^2, the bioavailability of molecule is decreased substantially [42]. In the present study, all molecules showed excellent TPSA values of < 60 Å^2 except compound **5h** and **5n** have shown slightly higher TPSA values but not exceeding the upper limit. Thus all these molecules have desirable drug-like TPSA property.

3. Conclusions

In conclusion, a series of novel hydrazones of 2, 3, 4,4a tetrahydroxanthene-1-one **(5a–n)** have been synthesized and screened them mainly for their in vitro α-glucosidase inhibition activity. Importantly, all the synthesized compounds are more active than the standard. Among the series, compounds **5l, 5g, 5j, 5n and 5m** are found to be the most active α-glucisidase inhibitors with IC_{50} values of 62.25 ± 0.11, 79.25 ± 0.15, 95.48 ± 0.13, 96.48 ± 0.53 and 96.54 ± 0.57 μM, respectively compared to standard acarbose (IC_{50} = 375.38 ± 0.12 μM). These results clearly indicate the potential of this class of compounds and highlight the significant role of substituents in biological activity. The ADME properties of all molecules showed excellent TPSA values of < 60 Å^2 except compound **5h** and **5n** that have shown slightly higher TPSA values but not exceeding the upper limit, so all these molecules have desirable drug-like TPSA property. Molecular modelling established the binding pattern of the more active compound **5l** and also emphasized the role of trifluoromethyl substituent in its potent α-glucisidase inhibitory activity. The highly active compounds presented in this manuscript provide an interesting platform for the development of drugs that can effectively be used for treatment of diabetes mellitus type II.

4. Experimental

4.1. General information

Melting points were taken on a Fisher-Johns melting point apparatus and are uncorrected. IR spectra (KBr discs) were take on Shimadzu Prestige-21 FT-IR spectrometer. The ^{1}H NMR spectra were recorded in $CDCl_3$ or DMSOd_6 on Bruker-500 MHz spectrometer, operating at 400 & 500 MHz and ^{13}C NMR at 125 MHz using TMS as an internal standard. The electron impact mass spectra (EIMS) were determined with JEOL MS Route mass spectrometer. TLC plates used to check the purity of compounds were coated with Merck silica gel 60 GF254. *In vitro* biological evaluation of the synthesized compounds was done at Department of Biochemistry and Biotechnology, The Islamia University of Bahawalpur, Bahawalpur.

4.2. Preparation of 2,3,4,4a,-tetrahydro-xanthene-1-one *(3)*

The precursor xanthene was prepared following our previously reported procedure [32]. Briefly, to a solution of salicylaldehyde (1 mmol) in methanol (3 mL) was added and trimethyl amine (1 mmol). After stirring at room temperature for 10 min, cyclohexene-1-one (3 mL) was added and the reaction mixture was stirred for 36 h at room temperature. After completion of the reaction as monitored by TLC, the orange yellow precipitate formed were filtered and washed with cold methanol and dried under vacuum to afford xanthene **1**.

4.3. Synthesis of Xanthene-hydrazones *(5a–n)*

A solution of the hydrazide **(4a–n)** (1 mmol) in ethanol (8 mL) was added cautiously to a stirred solution of 2,3,4,4a,-tetrahydro-xanthene-1-one **(3)** (1 mmol) in ethanol (8 mL) in the presence of acetic acid as catalyst (1–2 drops) and the reaction mixture was heated at reflux for 8 h. The progress of the reactions was monitored by TLC. After completion, yellow solid separated and the reaction was cooled at room temperature. The product was filtered, washed with cold ethanol and dried under vacuum. The synthesized hydrazone derivatives were further purified via recrystallization using ethanol/dioxan as solvent mixture. The spectral data of the hydrazones **(5a–n)** is given as under.

4.3.1. *(E)-N′-(2,3,4,4a-tetrahydro-1H-xanthen-1-ylidene)benzohydrazide (5a)*

Off-white solid, Yield, 84%; mp, 250–252 °C; IR (KBr), υ (cm^{-1}):

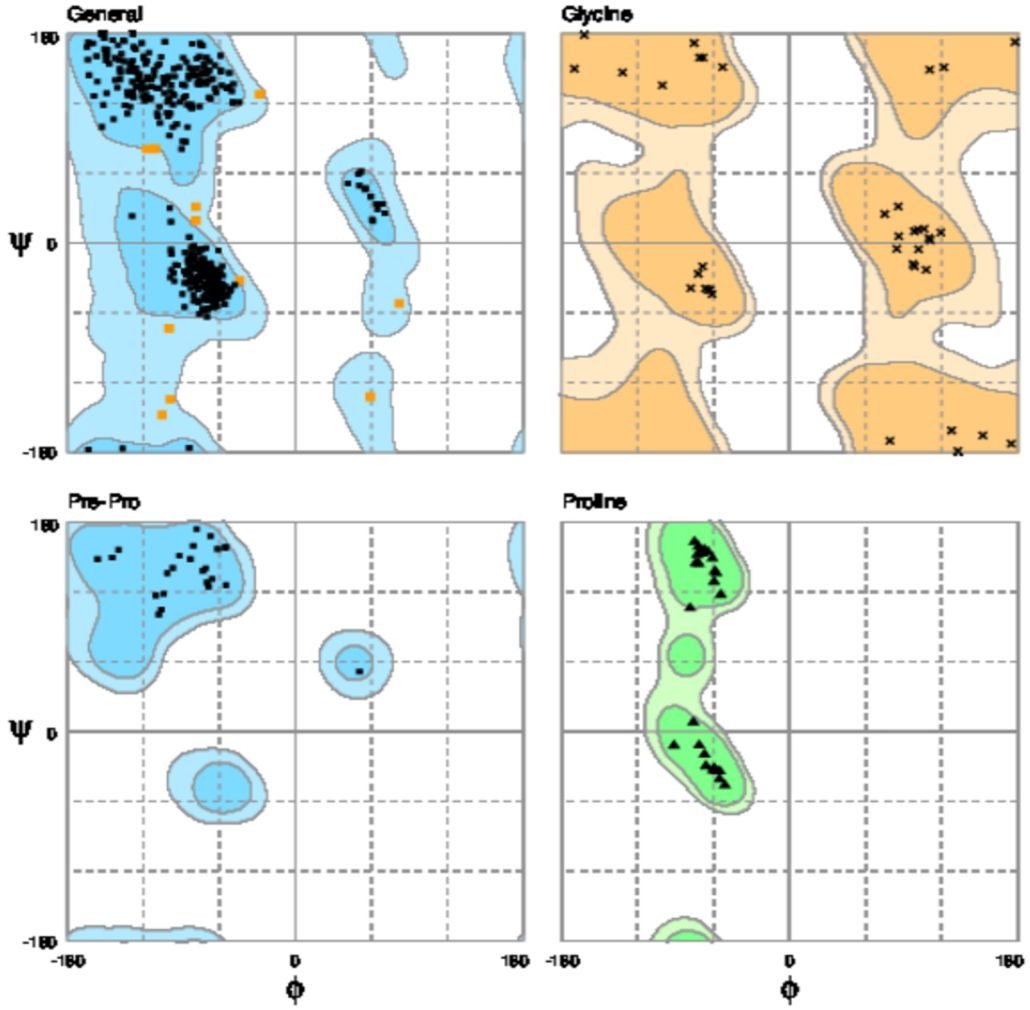

Fig. 7. Validation of homology model of α-glucosidase using RAMPAGE Ramachandran Plot.

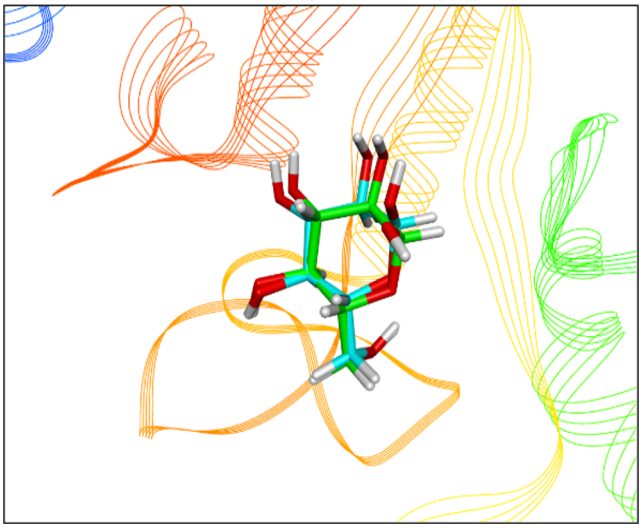

Fig. 8. Validation of docking protocol, co-crystal bound α-D-glucose (green) and redocked α-D-glucose (cyan) in model structure (RMSD = 0.73).

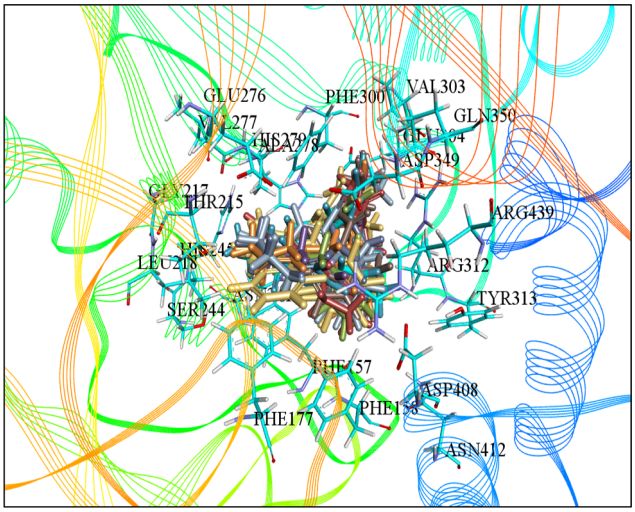

Fig. 9. Orientation of all docked compounds **(5a–n)**, within the active site of modelled structure of α-glucosidase. Different interacting amino acids within the active site of α-glucosidase are shown in stick form.

3305 (NH), 1681 (C=O), 1609 (C=N). ^{1}H NMR (DMSOd_6), δ (ppm): 1.46–1.50 (m, 1H, cyclohexyl), 1.75–1.83 (m, 1H, cyclohexyl), 1.88–1.95 (m, 1H, cyclohexyl), 2.09–2.24 (m, 2H, cyclohexyl), 2.70–2.78 (m, 1H, cyclohexyl), 4.83–4.88 (m, 1H, O−CH), 6.82–6.84 (m, 1H, *Ar*−*H*), 6.90–6.94 (m, 1H, *Ar*−*H*), 7.14–7.17 (m, 2H, *Ar*−*H*), 7.22–7.24 (m, 2H, *Ar*−*H*), 7.30–7.32 (m, 4H, *Ar*−*H*), 10.53 (s, 1H, NH−N); ^{13}C NMR δ (ppm) 18.47, 26.54, 29.86, 74.71, 115.69, 120.74, 121.56, 122.32, 123.66, 126.77, 128.68, 129.55, 130.01, 131.68,

Table 4
ChemGauss4 score of all compounds **(5a–n)** against α-glucosidase modelled structures.

Compound	ChemGauss4 score
5a	−11.09
5b	−10.49
5c	−10.77
5d	−10.42
5e	−10.61
5f	−11.03
5g	−10.94
5h	−11.55
5i	−11.29
5j	−10.84
5k	−11.04
5l	−11.47
5m	−11.76
5n	−7.77

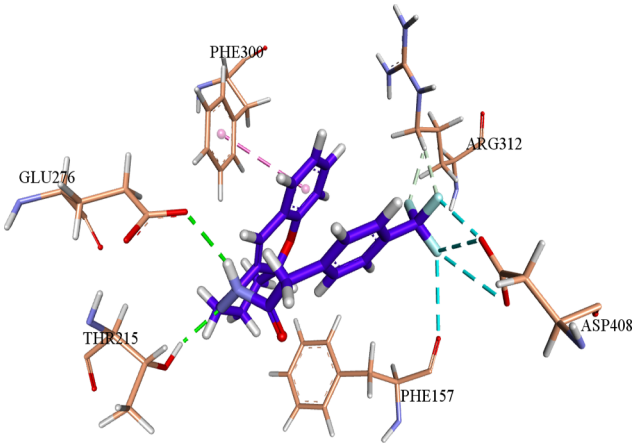

Fig. 10. 3D binding interactions of compound **5l** within the active site of α-glucosidase. Interacting amino acid residues are shown in light tan colour while compound is shown in blue colour. Hydrogen bonding is shown in green dotted form while pi-pi interaction is shown in pink dotted line, other halogen interactions are shown in cyan colour.

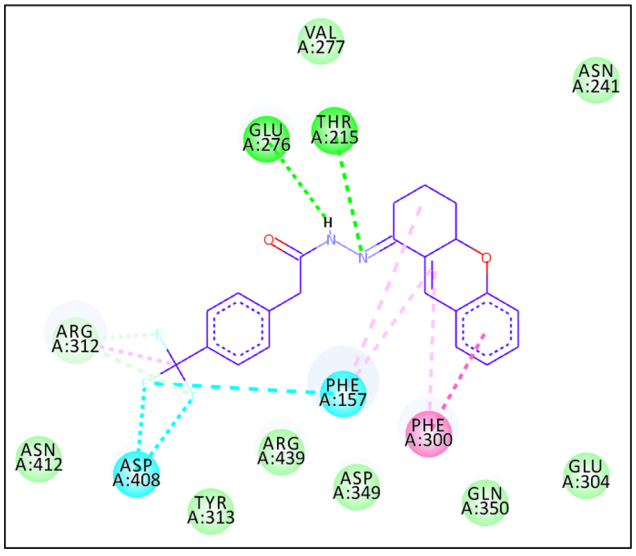

Fig. 11. 2D binding interactions of compound **5l** within the active site of α-glucosidase. Hydrogen bonding is shown in green dotted form while pi-pi interaction is shown in pink dotted line, other halogen interactions are shown in cyan colour.

Table 5
Calculated values of ADME properties of compounds.

Code	MlogP	S + logP	S + logD	Mol Wt	MNO	TPSA	HBDH
5a	3.445	4.009	4.007	318.378	4	50.69	1
5b	3.825	4.262	4.259	336.368	4	50.69	1
5c	4.204	4.582	4.579	354.359	4	50.69	1
5d	4.046	4.475	4.473	350.395	4	50.69	1
5e	4.046	4.583	4.581	350.395	4	50.69	1
5f	4.046	4.547	4.544	350.395	4	50.69	1
5g	4.046	4.554	4.552	350.395	4	50.69	1
5h	4.158	5.462	4.883	384.437	5	70.92	2
5i	2.430	2.895	2.892	319.365	5	63.58	1
5j	3.778	4.139	4.138	350.395	4	50.69	1
5k	3.778	4.205	4.204	350.395	4	50.69	1
5l	4.208	4.782	4.781	400.403	4	50.69	1
5m	3.992	5.275	5.274	426.519	5	59.92	1
5n	4.039	5.834	5.833	550.445	7	89.02	2

S + logP and MlogP are octanol-water distribution coefficients (It should be < 5.0).
S + logD is pH dependent octanol-water distribution coefficient.
HBDH indicates number of hydrogen bond donors (It should be < 5H-bond donors)
MNO value indicates total number of hydrogen bond acceptor (sum of N & O atoms).
It should be < 10H-bond acceptors.
Mol Wt is molecular weight (It should be 180–480 Daltons).
TPSA is the topological polar surface area expressed in square angstroms (It should be < 140 Å^2).

136.38, 146.83, 151.75, 154.48, 167.44, 173.59; HRMS calc. for $C_{20}H_{18}N_2O_2$ 318.1368, found 318.1371.

4.3.2. (E)-2-fluoro-N′-(2,3,4,4a-tetrahydro-1H-xanthen-1-ylidene) benzohydrazide ***(5b)***

White solid, Yield, 72%; mp, 208–209 °C; IR (KBr), υ (cm^{-1}): 3347 (NH), 1687 (C═O), 1610 (C═N). ^{1}H NMR ($CDCl_3$), δ (ppm): 1.52–1.63 (m, 1H, cyclohexyl), 1.85–1.94 (m, 1H, cyclohexyl), 2.11–2.16 (m, 2H, cyclohexyl), 2.31–2.34 (m, 1H, cyclohexyl), 2.52–2.57 (m, 1H, cyclohexyl), 4.83–4.87 (m, 1H, O−CH), 6.84 (d, 1H, J = 8.0 Hz, *Ar−H*), 6.92 (t, 1H, J = 6.8 Hz, *Ar−H*), 7.05–7.21 (m, 6H, *Ar−H*), 7.31–7.32 (m, 1H, *Ar−H*), 8.72 (s, 1H, NH−N); ^{13}C NMR δ (ppm) 18.44, 24.77, 29.44, 74.27, 115.19, 115.37, 115.59, 121.94, 122.22, 123.53, 124.06, 127.82, 128.74, 129.82, 129.98, 131.58, 131.61, 146.74, 154.55, 160.20, 162.16; HRMS calc. for $C_{20}H_{17}FN_2O_2$ 336.1274, found 336.1272.

4.3.3. (E)-3,4-difluoro-N′-(2,3,4,4a-tetrahydro-1H-xanthen-1-ylidene) benzohydrazide ***(5c)***

Light yellow solid, Yield, 80%; mp, 224–225 °C; IR (KBr), υ (cm^{-1}): 3332 (NH), 1647 (C═O), 1605 (C═N). ^{1}H NMR (DMSOd_6), δ (ppm): 1.44–1.54 (m, 1H, cyclohexyl), 1.74–1.83 (m, 1H, cyclohexyl), 1.88–1.92 (m, 1H, cyclohexyl), 2.07–2.25 (m, 2H, cyclohexyl), 2.71–2.78 (m, 1H, cyclohexyl), 4.85–4.87 (m, 1H, O−CH), 6.82–6.85 (m, 1H, *Ar−H*), 6.94 (t, 1H, J = 7.5 Hz, *Ar−H*), 7.11–7.25 (m, 4H, *Ar−H*), 7.34–7.38 (m, 2H, *Ar−H*), 10.61 (s, 1H, NH−N); ^{13}C NMR δ (ppm) 18.56, 26.55, 29.84, 74.69, 115.70, 117.70, 118.61, 119.03, 120.89, 121.66, 122.31, 123.63, 126.83, 128.14, 130.04, 131.58, 134.09, 147.17, 154.501, 166.88, 173.03; HRMS calc. for $C_{20}H_{16}F_2N_2O_2$ 354.1179, found 354.1183.

4.3.4. (E)-3-fluoro-2-methyl-N′-(2,3,4,4a-tetrahydro-1H-xanthen-1-ylidene)benzohydrazide ***(5d)***

Light yellow solid, Yield, 85%; mp, 222–224 °C; IR (KBr), υ (cm^{-1}): 3231 (NH), 1664 (C═O), 1606 (C═N). ^{1}H NMR (DMSOd_6), δ (ppm): 1.49–1.51 (m, 1H, cyclohexyl), 1.89–1.90 (m, 1H, cyclohexyl), 1.78–1.83 (m, 1H, cyclohexyl), 2.15–2.20 (m, 2H, cyclohexyl), 2.27 (s, 3H, CH_3), 2.78–2.81 (m, 1H, cyclohexyl), 4.91–4.93 (m, 1H, O−CH),

6.85 (d, 2H, J = 8.0 Hz, *Ar—H*), 6.95 (t, 1H, J = 7.5 Hz, *Ar—H*), 7.12–7.19 (m, 2H, *Ar—H*), 7.27–7.33 (m, 3H, *Ar—H*), 10.88 (s, 1H, NH—N); ^{13}C NMR δ (ppm) 11.80, 18.65, 26.90, 29.91, 74.74, 115.71, 116.86, 122.23, 123.12, 123.26, 123.64, 124.20, 127.81, 128.34, 130.31, 131.69, 138.66, 154.64, 161.99, 164.89, 171.22; HRMS calc. for $C_{21}H_{19}FN_2O_2$ 350.1430, found 350.1432.

4.3.5. (E)-3-fluoro-4-methyl-N′-(2,3,4,4a-tetrahydro-1H-xanthen-1-ylidene)benzohydrazide **(5e)**

Light brown solid, Yield, 80%; mp, 188–190 °C; IR (KBr), υ (cm^{-1}): 3370 (NH), 1675 (C═O), 1606 (C═N). ^{1}H NMR ($CDCl_3$), δ (ppm): 1.65–1.75 (m, 2H, cyclohexyl), 1.96–2.03 (m, 1H, cyclohexyl), 2.09–2.11 (m, 1H, cyclohexyl), 2.34 (s, 3H, CH_3), 2.56–2.62 (m, 2H, cyclohexyl), 4.91–4.93 (m, 1H, O—CH), 6.83–6.97 (m, 3H, *Ar—H*), 7.14–7.15 (m, 1H, *Ar—H*), 7.21–7.27 (m, 2H, *Ar—H*), 7.42–7.43 (m, 2H, *Ar—H*), 7.5 (bs, 1H, NH—N); ^{13}C NMR δ (ppm) 17.72, 29.53, 38.28, 74.80, 115.72, 116.13, 122.34, 122.40, 122.51, 123.57, 128.31, 130.25, 130.32, 130.38, 131.36, 131.80, 132.46, 153.88, 155.77, 197.11; HRMS calc. for $C_{21}H_{19}FN_2O_2$ 350.1430, found 350.1433.

4.3.6. (E)-2-fluoro-5-methyl-N′-(2,3,4,4a-tetrahydro-1H-xanthen-1-ylidene)benzohydrazide **(5f)**

Brown solid, Yield, 65%; mp, 194–196 °C; IR (KBr), υ (cm^{-1}): 3293 (NH), 1667 (C═O), 1623 (C═N). ^{1}H NMR (DMSOd_6), δ (ppm): 1.50–1.54 (m, 1H, cyclohexyl), 1.81–1.90 (m, 2H, cyclohexyl), 2.21–2.27 (m, 2H, cyclohexyl), 2.33 (s, 3H, CH_3), 2.78–2.81 (m, 1H, cyclohexyl), 4.90–4.93 (m, 1H, O—CH), 6.81–6.98 (m, 3H, *Ar—H*), 7.17–7.30 (m, 4H, *Ar—H*), 7.47–7.88 (m, 1H, *Ar—H*), 10.77 (s, 1H, NH—N); ^{13}C NMR δ (ppm) 18.62, 20.49, 26.70, 29.89, 74.71, 115.72, 116.19, 122.27, 123.62, 128.34, 130.38, 131.61, 132.45, 133.43, 134.17, 147.90, 154.32, 157.06, 159.01, 161.18, 168.59, 197.10; HRMS calc. for $C_{21}H_{19}FN_2O_2$ 350.1430, found 350.1432.

4.3.7. (E)-4-fluoro-3-methyl-N′-(2,3,4,4a-tetrahydro-1H-xanthen-1-ylidene)benzohydrazide **(5g)**

Light yellow solid, Yield, 79%; mp, 190–191 °C; IR (KBr), υ (cm^{-1}): 3352 (NH), 1653 (C═O), 1608 (C═N). ^{1}H NMR ($CDCl_3$), δ (ppm): 1.60–1.69 (m, 1H, cyclohexyl), 1.91–2.00 (m, 1H, cyclohexyl), 2.08–2.12 (m, 1H, cyclohexyl), 2.34 (s, 3H, CH_3), 2.31–2.36 (m, 2H, cyclohexyl), 2.66–2.70 (m, 1H, cyclohexyl), 4.88 (m, 1H, O—CH), 6.84 (d, 1H, J = 8.0 Hz, *Ar—H*), 6.92 (ddd, 1H, J = 7.6, 0.8 Hz, *Ar—H*), 7.08 (t, 1H, J = 8.8 Hz, *Ar—H*), 7.13–7.18 (m, 2H, *Ar—H*), 7.62–7.73 (m, 2H, *Ar—H*), 8.38 (s, 1H, NH—N); ^{13}C NMR δ (ppm) 14.57, 18.61, 29.66, 38.82, 74.11, 115.52, 116.02, 121.72, 123.36, 124.23, 126.52, 128.14, 129.82, 130.01, 131.53, 132.06, 154.60, 162.57, 164.55, 197.54; HRMS calc. for $C_{21}H_{19}FN_2O_2$ 350.1430, found 350.1434.

4.3.8. (E)-2-hydroxy-N′-(2,3,4,4a-tetrahydro-1H-xanthen-1-ylidene)-1-naphthohydrazide **(5h)**

Yellow solid, Yield, 88%; mp, 228–229 °C; IR (KBr), υ (cm^{-1}): 3205 (NH), 1674 (C═O), 1617 (C═N). ^{1}H NMR (DMSOd_6), δ (ppm): 1.58–1.64 (m, 1H, cyclohexyl), 1.83–1.90 (m, 1H, cyclohexyl), 1.97–1.99 (m, 1H, cyclohexyl), 2.27–2.30 (m, 1H, cyclohexyl), 2.36–2.40 (m, 1H, cyclohexyl), 2.73–2.77 (m, 1H, cyclohexyl), 4.91–4.94 (m, 1H, O—CH), 6.88 (d, 1H, J = 8.0 Hz, *Ar—H*), 6.96 (t, 1H, J = 7.5 Hz, *Ar—H*), 7.19 (t, 1H, J = 7.0 Hz, *Ar—H*), 7.32–7.38 (m, 4H, *Ar—H*), 7.50 (t, 1H, J = 7.5 Hz, *Ar—H*), 7.77 (d, 1H, J = 8.0 Hz, *Ar—H*), 8.64 (s, 1H, *Ar—H*), 11.51 (s, 1H, OH), 11.75 (s, 1H, NH—N); ^{13}C NMR δ (ppm) 18.47, 26.09, 29.54, 74.60, 111.14, 115.75, 121.13, 122.01, 122.40, 123.77, 124.39, 126.18, 127.68, 128.38, 128.79, 129.41, 130.31, 131.33, 132.79, 136.23, 151.95, 153.11, 154.63, 161.75; HRMS calc. for $C_{24}H_{20}N_2O_3$ 384.1473, found 384.1474.

4.3.9. (E)-N′-(2,3,4,4a-tetrahydro-1H-xanthen-1-ylidene) nicotinohydrazide **(5i)**

Light brown solid, Yield, 80%; mp, 186–187 °C; IR (KBr), υ (cm^{-1}): 3213 (NH), 1666 (C═O), 1602 (C═N). ^{1}H NMR (DMSOd_6), δ (ppm): 1.50–1.55 (m, 1H, cyclohexyl), 1.83–1.85 (m, 1H, cyclohexyl), 1.93–1.95 (m, 1H, cyclohexyl), 2.27–2.29 (m, 2H, cyclohexyl), 2.88–2.93 (m, 1H, cyclohexyl), 4.93–4.95 (m, 1H, O—CH), 6.86 (d, 1H, J = 8.0 Hz, *Ar—H*), 6.93–6.98 (m, 1H, *Ar—H*), 7.17–7.23 (m, 3H, *Ar—H*), 7.53–7.55 (m, 1H, *Ar—H*), 8.21 (d, 1H, J = 7.5 Hz, *Ar—H*), 8.74 (s, 1H, *Ar—H*), 9.01 (s, 1H, *Ar—H*), 10.95 (s, 1H, NH—N); ^{13}C NMR δ (ppm) 18.74, 26.99, 29.53, 74.74, 115.73, 116.13, 122.35, 123.55, 128.36, 130.25, 131.70, 132.46, 136.18, 149.23, 152.50, 154.66, 155.77, 156.02, 162.90; HRMS calc. for $C_{19}H_{17}N_3O_2$ 319.1320, found 319.1324.

4.3.10. (E)-2-(3-fluorophenyl)-N′-(2,3,4,4a-tetrahydro-1H-xanthen-1-ylidene)acetohydrazide **(5j)**

Off-white solid, Yield, 73%; mp, 206–207 °C; IR (KBr), υ (cm^{-1}): 3378 (NH), 1665 (C═O), 1602 (C═N). ^{1}H NMR ($CDCl_3$), δ (ppm): 1.56–1.63 (m, 1H, cyclohexyl), 1.88–1.91 (m, 1H, cyclohexyl), 2.07–2.15 (m, 2H, cyclohexyl), 2.31–2.35 (m, 1H, cyclohexyl), 2.51–2.56 (m, 1H, cyclohexyl), 4.09 (s, 2H, CH_2—C═O), 4.83–4.88 (m, 1H, O—CH), 6.86 (d, 1H, J = 8.4 Hz, *Ar—H*), 6.93–6.97 (m, 2H, *Ar—H*), 7.12–7.17 (m, 5H, *Ar—H*), 7.28–7.30 (m, 1H, *Ar—H*), 8.70 (s, 1H, NH—N); ^{13}C NMR δ (ppm) 18.46, 25.86, 26.55, 29.65, 74.69, 113.50, 115.68, 120.85, 122.32, 125.73, 126.13, 128.11, 130.61, 131.72, 139.20, 147.08, 151.95, 154.49, 161.52, 166.93, 173.10; HRMS calc. for $C_{21}H_{19}FN_2O_2$ 350.1430, found 350.1434; EIMS (70 eV) *m/z*: 350, 331, 304, 281, 231, 214, 213, 199, 198, 169, 157, 131, 109, 83, 69.

4.3.11. (E)-2-(4-fluorophenyl)-N′-(2,3,4,4a-tetrahydro-1H-xanthen-1-ylidene)acetohydrazide **(5k)**

Light yellow solid, Yield, 85%; mp, 225–226 °C; IR (KBr), υ (cm^{-1}): 3342 (NH), 1666 (C═O), 1611 (C═N). ^{1}H NMR ($CDCl_3$), δ (ppm): 1.57–1.62 (m, 1H, cyclohexyl), 1.85–1.95 (m, 1H, cyclohexyl), 2.07–2.17 (m, 2H, cyclohexyl), 2.32–2.36 (m, 1H, cyclohexyl), 2.51–2.56 (m, 1H, cyclohexyl), 4.07 (s, 2H, CH_2—C═O), 4.83–4.88 (m, 1H, O—CH), 6.87 (d, 1H, J = 7.6 Hz, *Ar—H*), 6.95 (ddd, 1H, J = 1.2, 7.6 Hz, *Ar—H*), 7.01 (t, 1H, J = 8.4 Hz, *Ar—H*), 7.15–7.17 (m, 2H, *Ar—H*), 7.20 (m, 1H, *Ar—H*), 7.30–7.33 (m, 2H, *Ar—H*), 8.65 (s, 1H, NH—N); ^{13}C NMR δ (ppm) 18.42, 24.71, 29.40, 38.72, 74.23, 115.25, 122.00, 122.19, 123.42, 127.80, 129.82, 130.55, 131.06, 131.12, 131.52, 132.05, 146.65, 154.58, 160.92, 162.87, 173.39; HRMS calc. for $C_{21}H_{19}FN_2O_2$ 350.1430, found 350.1433.

4.3.12. (E)-N′-(2,3,4,4a-tetrahydro-1H-xanthen-1-ylidene)-2-(4-(trifluoromethyl)phenyl) acetohydrazide **(5l)**

Yellow solid, Yield, 82%; mp, 188–190 °C; IR (KBr), υ (cm^{-1}): 3370 (NH), 1675 (C═O), 1620 (C═N). ^{1}H NMR ($CDCl_3$), δ (ppm): 1.57–1.61 (m, 1H, cyclohexyl), 1.85–1.95 (m, 1H, cyclohexyl), 2.07–2.18 (m, 2H, cyclohexyl), 2.31–2.36 (m, 1H, cyclohexyl), 2.51–2.56 (m, 1H, cyclohexyl), 4.16 (s, 2H, CH_2—C═O), 4.84–4.88 (m, 1H, O—CH), 6.87 (d, 1H, J = 8.4 Hz, *Ar—H*), 6.95 (t, 1H, J = 7.2 Hz, *Ar—H*), 7.15–7.21 (m, 3H, *Ar—H*), 7.47 (d, 2H, J = 7.6 Hz, *Ar—H*), 7.59 (d, 2H, J = 8.0 Hz, *Ar—H*), 8.72 (s, 1H, NH—N); ^{13}C NMR δ (ppm) 18.57, 25.91, 26.57, 29.84, 74.68, 115.69, 120.92, 121.69, 122.31, 123.82, 125.59, 128.20, 130.89, 131.57, 141.37, 147.28, 152.06, 154.54, 166.77, 172.98; HRMS calc. for $C_{22}H_{19}F_3N_2O_2$ 400.1398, found 400.1400.

4.3.13. (E)-2-(6-methoxynaphthalen-2-yl)-N′-(2,3,4,4a-tetrahydro-1H-xanthen-1-ylidene) propanehydrazide **(5m)**

Orange crystalline solid, Yield, 90%; mp, 250–251 °C; IR (KBr), υ (cm^{-1}): 3368 (NH), 1668 (C═O), 1609 (C═N). ^{1}H NMR (DMSOd_6), δ (ppm): 1.45 (d, 3H, J = 7.0 Hz, CH-CH_3), 1.64–1.73 (m, 1H, cyclohexyl), 1.91–1.94 (m, 2H, cyclohexyl), 2.36–2.37 (m, 1H, cyclohexyl), 2.41–2.42 (m, 2H, cyclohexyl), 3.86 (s, 3H, OCH_3), 3.90 (q, 1H, CH_3—CH), 5.01–5.04 (m, 1H, O—CH), 6.91 (d, 1H, J = 8.0 Hz, *Ar—H*), 6.98 (ddd, 1H, J = 1.0, 7.5 Hz, *Ar—H*), 7.15 (dd, 1H, J = 2.5, 8.5 Hz, *Ar—H*), 7.27–7.30 (m, 2H, *Ar—H*), 7.36–7.41 (m, 3H, *Ar—H*), 7.71 (bs,

Table 6
Crystallographic data of compound **5g**.

Crystal data	Compound 5g
CCDC	**1868047**
Chemical formula	$C_{21}H_{19}FN_2O_2$
M_r	350.38
Crystal system, space group	Orthorhombic, *Pbca*
Temperature (K)	296
a, *b*, *c* (Å)	10.9507 (12), 8.4035 (9), 38.145 (5)
V (Å^3)	3510.2 (7)
Z	8
Radiation type	Mo *K*α
μ (mm^{-1})	0.09
Crystal size (mm)	0.45 × 0.38 × 0.32
Data collection	
Diffractometer	Bruker Kappa APEXII CCD
Absorption correction	Multi-scan (*SADABS*; Bruker, 2005)
T_{min}, T_{max}	0.940, 0.980
No. of measured, independent and observed [$I > 2\sigma(I)$] reflections	16392, 4162, 2236
R_{int}	0.068
(sin θ/λ)$_{max}$ (Å^{-1})	0.658
Refinement	
$R[F^2 > 2\sigma(F^2)]$, $wR(F^2)$, *S*	0.073, 0.196, 1.02
No. of reflections	4162
No. of parameters	234
No. of restraints	18
H-atom treatment	H-atom parameters constrained
$\Delta\rangle_{max}$, $\Delta\rangle_{min}$ (e Å^{-3})	0.25, −0.21

1H, NH—N), 7.70–7.80 (m, 2H, *Ar—H*); ^{13}C NMR *δ* (ppm) 14.47, 18.96, 29.53, 38.85, 44.91, 60.70, 74.80, 106.18, 116.12, 119.23, 122.40, 122.50, 126.04, 126.64, 127.46, 128.86, 129.61, 130.25, 131.35, 132.45, 133.78, 136.25, 155.77, 157.66, 174.38, 197.10; HRMS calc. for $C_{27}H_{26}N_2O_3$ 426.1943, found 426.1944.

4.3.14. (E)-2-oxo-2-(2-(2,3,4,4a-tetrahydro-1H-xanthen-1-ylidene) hydrazinyl)ethyl2-(2-((2,6-dichlorophenyl)amino)phenyl)acetate (5n)

Orange solid, Yield, 81%; mp, 236–237 °C; IR (KBr), *υ* (cm^{-1}): 3371, 3345 (NH), 1652 (C═O), 1611 (C═N). ^{1}H NMR (DMSOd_6), *δ* (ppm): 1.66–1.70 (m, 1H, cyclohexyl), 1.92–1.97 (m, 2H, cyclohexyl), 2.36–2.37 (m, 1H, cyclohexyl), 2.41–2.43 (m, 2H, cyclohexyl), 3.89 (s, 4H, 2xCH_2), 5.01–5.03 (m, 1H, O—CH), 6.38 (d, 1H, *J* = 8.0 Hz, *Ar—H*), 6.89 (d, 1H, *J* = 8.0 Hz, *Ar—H*), 6.98 (ddd, 1H, *J* = 0.5, 7.5 Hz, *Ar—H*), 7.09 (t, 2H, *J* = 7.5 Hz, *Ar—H*), 7.21 (t, 2H, *J* = 7.5 Hz, *Ar—H*), 7.28 (ddd, 2H, *J* = 1.5, 8.0 Hz, *Ar—H*), 7.37–7.41 (m, 3H, *Ar—H*), 7.61 (t, 1H, *J* = 8.0 Hz, *Ar—H*), 7.44 (s, 1H, NH), 7.61 (s, 1H, NH—N); ^{13}C NMR *δ* (ppm) 17.73, 29.53, 35.55, 38.85, 74.80, 108.97, 116.12, 122.40, 122.49, 123.30, 125.08, 125.46, 128.28, 129.84, 130.26, 130.37, 131.34, 132.37, 132.44, 134.92, 143.27, 155.77, 173.69, 197.08; HRMS calc. for $C_{29}H_{25}Cl_2N_3O_4$ 549.1222, found 549.1224.

4.4. Structural refinement and crystallographic data collection

The structural refinement and protocol for crystallographic data collection were followed as reported previously [32,36]. The refinement values of compound **5g** and crystal data are summarized in Table 6.

4.5. In silico Studies

4.5.1. Homology modelling of S. cerevisiae α- glucosidase

Homology model of α-glucosidase from *S. cerevisiae* was built because till date no crystal structure of α-glucosidase was reported in Protein Database Bank (PDB). Amino acid sequence of α-glucosidase was retrieved using UniProt ID P53341 and aligned with best selected template of isomaltase from *S. cerevisiae* (PDB ID: 3A4A) http://www.uniprot.org/uniprot/P53341 [48]. Sequence alignment was carried using "zAlign sequence to template" tool in Discovery Studio Client vs 16.1 program (Accelrys Software Inc., 2016)) and homology modelling was also performed using built-in MODELER v9.15 in DS software [47]. Best homology model was selected based on DOPE score while validation and assessment were conducted via Ramachandran plot using RAMPAGE [49].

4.5.2. Molecular Docking Studies

Molecular Docking calculations were performed using FRED tool in Open Eye software [43,44] All compounds were first drawn in Chemdraw Professionals version 15.1 and then imported into Discovery Studio for 3D structure generation and energy minimization. OMEGA 2.5 tool of OpenEye Scientific was used for generation of conformers of compounds [45,46]. Active site was selected based on modelled co-crystal ligand α-D-glucose. Before molecular docking studies, docking protocol was optimized for co-crystal ligand and then final docking was carried out for all compounds as well as reference compound for comparison. During docking calculations, twenty different poses were generated and sorted out based on the lowest ChemGauss4 score. Binding orientations were also visualized using Discovery Studio software [47].

Acknowledgments

Z. Shafiq is thankful to BZ University, Multan, Pakistan for providing financial support. Shafi Ullah Khan wish to thank OpenEye Scientific Software for providing a free academic license.

Appendix A. Supplementary material

Supplementary data to this article can be found online at https://doi.org/10.1016/j.bioorg.2018.11.053.

References

[1] J.D. Sunderhaus, S.F. Martin, Applications of multicomponent reactions to the synthesis of diverse heterocyclic scaffolds, Chem. Eur. J. 15 (2009) 1300–1308.
[2] R.M.N. Kalla, A. Varyambath, M.R. Kim, I. Kim, Amine-functionalized hyper-crosslinked polyphenanthrene as a metal-free catalyst for the synthesis of 2-amino-tetrahydro-4H-chromene and pyran derivatives, Appl. Catal. A 538 (2017) 9–18.
[3] J.M. Khurana, A. Chaudhary, A. Lumb, B. Nand, Efficient one-pot syntheses of dibenzo [a, i] xanthene-diones and evaluation of their antioxidant activity, Can. J. Chem. 90 (2012) 739–746.
[4] Y. Liu, L. Ma, W.-H. Chen, B. Wang, Z.-L. Xu, Synthesis of xanthone derivatives with extended π-systems as α-glucosidase inhibitors: insight into the probable binding mode, Bioorg. Med. Chem. 15 (2007) 2810–2814.
[5] H. Wang, L. Lu, S. Zhu, Y. Li, W. Cai, The phototoxicity of xanthene derivatives against *Escherichia coli*, *Staphylococcus aureus*, and *Saccharomyces cerevisiae*, Curr. Microbiol. 52 (2006) 1–5.
[6] Y.-F. Qiao, T. Okazaki, T. Ando, K. Mizoue, K. Kondo, T. Eguchi, K. Kakinuma, Isolation and characterization of a new pyrano [4′,3′: 6,7] naphtho [1,2-b] xanthene antibiotic FD-594, J. Antibiot. 51 (1998) 282–287.
[7] S. Limsuwan, E.N. Trip, T.R. Kouwen, S. Piersma, A. Hiranrat, W. Mahabusarakam, S.P. Voravuthikunchai, J.M. van Dijl, O. Kayser, Rhodomyrtone: a new candidate as natural antibacterial drug from *Rhodomyrtus tomentosa*, Phytomedicine 16 (2009) 645–651.
[8] M. Kaya, E. Basar, F. Colak, Synthesis and antimicrobial activity of some bisocta-hydroxanthene-1,8-dione derivatives, Med. Chem. Res. 20 (2011) 1214–1219.
[9] A. Chaudhary, J.M. Khurana, Advances in the synthesis of xanthenes: an overview, Curr. Org. Synth. 15 (2018) 341–369.
[10] T. Nishiyama, K. Sakita, T. Fuchigami, T. Fukui, Antioxidant activities of fused heterocyclic compounds, xanthene-2,7-diols with BHT or catechol skeleton, Polym. Degrad. Stab. 62 (1998) 529–534.
[11] A.A. Bartolomeu, M. Menezes, L. Silva Filho, Efficient one-pot synthesis of 14-aryl-14H-dibenzo [a,j] xanthene derivatives promoted by niobium pentachloride, Chem. Pap. 68 (2014) 1593–1600.
[12] A. Banerjee, A. Mukherjee, Chemical aspects of santalin as a histological stain, Stain. Technol. 56 (1981) 83–85.
[13] M. Ahmad, T.A. King, D.-K. Ko, B.H. Cha, J. Lee, Performance and photostability of xanthene and pyrromethene laser dyes in sol-gel phases, J. Phys. D: Appl. Phys. 35 (2002) 1473.
[14] R.C. Hunter, T.J. Beveridge, Application of a pH-sensitive fluoroprobe (C-SNARF-4)

for pH microenvironment analysis in *Pseudomonas aeruginosa* biofilms, Appl. Environ. Microbiol. 71 (2005) 2501–2510.
[15] M. Torneiro, W.C. Still, Sequence-selective binding of peptides in water by a synthetic receptor molecule, J. Am. Chem. Soc. 117 (1995) 5887–5888.
[16] J.P. Poupelin, G. Saint-Ruf, J.C. Perche, J.C. Roussey, B. Laude, G. Narcisse, F. Bakri-Logeais, F. Hubert, 2-hydroxy-1, 3-indandione derivatives. II. Condensation products of ninhydrine with polyphenols and their o-methylated derivatives, Chem. Inf. 11 (1980).
[17] S.B. Krasnoff, D. Faloon, J.E. Williams, D.M. Gibson, Toxicity of xanthene dyes to entomopathogenic fungi, Biocontrol Sci. Technol. 9 (1999) 215–225.
[18] J. Kinjo, H. Uemura, T. Nohara, M. Yamashita, N. Marubayashi, K. Yoshihira, Novel yellow pigment from pterocarpus santalinus: biogenetic hypothesis for santalin analogs, Tetrahedron Lett. 36 (1995) 5599–5602.
[19] P. Jagadeesh, M. Himajaa, S.V. Malib, A. Ranjitha, A. Karigarc, M. Sikarward, Synthesis and antioxidant activity of novel ketone hydrazones bearing 5-(Pyridine-3-yl)-1,3,4-thiadiazole, J. Pharm. Res. 3 (2010) 2460–2462.
[20] K. Padmini, P.J. Preethi, M. Divya, P. Rohini, M. Lohita, K. Swetha, P. Kaladar, A review on biological importance of hydrazones, Int. J. Pharm. Res. Rev 2 (2013) 43–58.
[21] P. Vicini, M. Incerti, I.A. Doytchinova, P. La Colla, B. Busonera, R. Loddo, Synthesis and antiproliferative activity of benzo [d] isothiazole hydrazones, Eur. J. Med. Chem. 41 (2006) 624–632.
[22] N. Kumar, L. Chauhan, Analgesic and anti-inflammatory potential of hydrazones, J. Chem. Pharm. Res. 6 (2014) 916–934.
[23] P. Vicini, M. Incerti, P. La Colla, R. Loddo, Anti-HIV evaluation of benzo [d] isothiazole hydrazones, Eur. J. Med. Chem. 44 (2009) 1801–1807.
[24] M. Singh, N. Raghav, Biological activities of hydrazones: a review, Int. J. Pharm. Pharm. Sci. 3 (2011) 26–32.
[25] S. Constantin, A. Pânzariu, I. Vasincu, M. Apotrosoaei, L. Confederat, F. Buron, S. Routier, L. Profire, Synthesis and evaluation of antioxidant activity of some hydrazones with xanthine structure, Med. Surg. J. 119 (2015) 910–916.
[26] A. Kheradmand, L. Navidpour, H. Shafaroodi, G. Saeedi-Motahar, A. Shafiee, Design and synthesis of niflumic acid-based N-acylhydrazone derivatives as novel anti-inflammatory and analgesic agents, Med. Chem. Res. 22 (2013) 2411–2420.
[27] B. Elya, K. Basah, A. Mun'im, W. Yuliastuti, A. Bangun, E.K. Septiana, Screening of α-glucosidase inhibitory activity from some plants of apocynaceae, clusiaceae, euphorbiaceae, and rubiaceae, Biomed. Res. Int. 2012 (2011).
[28] H. King, R.E. Aubert, W.H. Herman, Global burden of diabetes, 1995–2025: prevalence, numerical estimates, and projections, Diabetes care 21 (1998) 1414–1431.
[29] K.G.M.M. Alberti, P.F. Zimmet, Definition, diagnosis and classification of diabetes mellitus and its complications. Part 1: diagnosis and classification of diabetes mellitus. Provisional report of a WHO consultation, Diabet. Med. 15 (1998) 539–553.
[30] K. Nakagawa, Studies targeting α-glucosidase inhibition, antiangiogenic effects, and lipid modification regulation: background, evaluation, and challenges in the development of food ingredients for therapeutic purposes, Biosci. Biotechnol. Biochem. 77 (2013) 900–908.
[31] A.D. Chougale, V.A. Ghadyale, S.N. Panaskar, A.U. Arvindekar, Alpha glucosidase inhibition by stem extract of *Tinospora cordifolia*, J. Enzyme. Inhib. Med. Chem. 24 (2009) 998–1001.
[32] A. Hameed, Z. Shafiq, M. Yaqub, M. Hussain, M.A. Hussain, M. Afzal, M.N. Tahir, M.M. Naseer, Me 3 N-promoted synthesis of 2,3,4,4a-tetrahydroxanthen-1-one: preparation of thiosemicarbazone derivatives, their solid state self-assembly and antimicrobial properties, New J. Chem. 39 (2015) 9351–9357.
[33] A. Hameed, M. Yaqub, M. Hussain, A. Hameed, M. Ashraf, H. Asghar, M.M. Naseer, K. Mahmood, M. Muddassar, M.N. Tahir, Coumarin-based thiosemicarbazones as potent urease inhibitors: synthesis, solid state self-assembly and molecular docking, RSC Adv. 6 (2016) 63886–63894.
[34] M. Islam, Z. Shafiq, M. Hussain, H.B. Ahmad, M.A. Hussain, Synthesis, characterization and antimicrobial studies of imine derivatives of amoxicillin, Eur. J. Chem. 6 (2015) 417–421.
[35] S. Naseem, M. Khalid, M.N. Tahir, M.A. Halim, A.A. Braga, M.M. Naseer, Z. Shafiq, Synthesis, structural, DFT studies, docking and antibacterial activity of a xanthene based hydrazone ligand, J. Mol. Struct. 1143 (2017) 235–244.
[36] R. Jawaria, M. Hussain, Z. Shafiq, H.B. Ahmad, M.N. Tahir, H.A. Shad, M.M. Naseer, Robustness of thioamide dimer synthon, carbon bonding and thioamide–thioamide stacking in ferrocene-based thiosemicarbazones, CrystEngComm 17 (2015) 2553–2561.
[37] M. Ahmad, H. Pervez, T.B. Hadda, L. Toupet, M.M. Naseer, Synthesis and solid state self-assembly of an isatin–thiazoline hybrid driven by three self-complementary dimeric motifs, Tetrahedron Lett. 55 (2014) 5400–5403.
[38] M. Yoshikawa, T. Morikawa, H. Matsuda, G. Tanabe, O. Muraoka, Absolute stereostructure of potent α-glucosidase inhibitor, salacinol, with unique thiosugar sulfonium sulfate inner salt structure from *Salacia reticulata*, Bioorg. Med. Chem. 10 (2002) 1547–1554.
[39] Y. Wang, L. Ma, Z. Li, Z. Du, Z. Liu, J. Qin, X. Wang, Z. Huang, L. Gu, A.S. Chen, Synergetic inhibition of metal ions and genistein on α-glucosidase, FEBS Lett. 576 (2004) 46–50.
[40] N.T. Patil, S. John, S.G. Sabharwal, D.D. Dhavale, 1-Aza-sugars from d-glucose. Preparation of 1-deoxy-5-dehydroxymethyl-nojirimycin, its analogues and evaluation of glycosidase inhibitory activity, Bioorg. Med. Chem. 10 (2002) 2155–2160.
[41] < http://www.simulations-plus.com > MedChem Designer, Simulation Plus Inc., California, USA. Ver. 3.0. 2014.
[42] P. Zakeri-Milani, H. Tajerzadeh, Z. Islambolchilar, S. Barzegar, H. Valizadeh, The relation between molecular properties of drugs and their transport across the intestinal membrane, DARU J. Pharm. Sci. 14 (2006) 164–171.
[43] M. McGann, FRED and HYBRID docking performance on standardized datasets, J. Comput. Aided Mol. Des. 26 (2012) 897–906.
[44] O. Toolkit, OpenEye Scientific Software, Santa Fe, NM, 2012.
[45] P.C. Hawkins, A.G. Skillman, G.L. Warren, B.A. Ellingson, M.T. Stahl, Conformer generation with OMEGA: algorithm and validation using high quality structures from the protein databank and Cambridge structural database, J. Chem. Inf. Model. 50 (2010) 572–584.
[46] P. Hawkins, A. Skillman, G. Warren, B. Ellingson, M. Stahl, OMEGA 2.5. 1.4, OpenEye Scientific Software, Santa Fe, NM, 2015.
[47] D.S. Biovia, BIOVIA Discovery Studio 2017 R2: a comprehensive predictive science application for the Life Sciences, San Diego, CA, USA, < http://accelrys.com/products/collaborative-science/biovia-discovery-studio > , 2017.
[48] K. Yamamoto, H. Miyake, M. Kusunoki, S. Osaki, Crystal structures of isomaltase from *Saccharomyces cerevisiae* and in complex with its competitive inhibitor maltose, FEBS J. 277 (2010) 4205–4214.
[49] S.C. Lovell, I.W. Davis, W.B. Arendall III, P.I. De Bakker, J.M. Word, M.G. Prisant, J.S. Richardson, D.C. Richardson, Structure validation by Cα geometry: ϕ, ψ and Cβ deviation, Proteins 50 (2003) 437–450.